Target Localization by Mobile Handheld UHF RFID Reader

Aristidis Raptopoulos Chatzistefanou*, Spyros Megalou*, Stavroula Siachalou*, Vasiliki Drakaki†, George D. Sergiadis*, Antonis G. Dimitriou*
*School of ECE, AUTH, Thessaloniki, Greece, antodimi@ece.auth.gr
†Archaelogical Museum of Thessaloniki, Thessaloniki, Greece, drvasilikh@gmail.com

***Abstract*—In this paper we design and implement a mobile handheld human operated device used to guide the user towards the desired RFID target, and at the same time provide estimations of the distance and the angle from the user to the target. The main components of the device are a UHF RFID reader operating with one antenna, and an IMU used to measure rotation angles. The user is instructed by the device to perform one of three different actions: SCAN, TURN and MOVE. During these actions phase of arrival and rotation angle data are collected by the RFID reader and the IMU respectively. A particle filter algorithm leverages the collected data to estimate the distance and angle of the user, with respect to the user's current pose. Experimental results show a mean angle estimation error of $\sim 4^o$, and distance estimation error less than $0.5m$ when the user approaches the target.**

***Index Terms*—RFID, handheld, phase, localization.**

I. Introduction

The penetration of Radio Frequency Identification (RFID) technology in health care, logistics, and security market has been rapid in the last decade. New RFID applications begin to emerge in various fields, aiming to provide services like assisted living, or enhanced and personalised user related experiences.

In this paper, we propose and construct a handheld UHF RFID reader, capable to guide the user towards a specific tag. The proposed device uses RFID technology to estimate the location of the target RFID tag relative to the user's pose. The prototype is developed in the context of project "CultureID", where we install UHF RFID technology inside the Archaeological Museum of Thessaloniki, Greece. An RFID tag is assigned to every exhibit. The proposed reader will be used as a "tool" in the context of games, developed for younger visitors inside the museum, guiding the visitors to the proper exhibit, to discover a hint related to a riddle, according to the game's script. However, the proposed device can be widely adopted for locating misplaced items in retail; a process currently being carried out by increasing/decreasing the sound of a beeper from a handheld reader, depending on the measured backscattered power.

Prior art consists of works in which data are collected by a mobile measuring system, or others sources that can communicate with it. Leveraging the collected data allows to calculate the position of the desired target relatively to the mobile agent.

Regarding RFID technology, various features of the received signal are used to locate the target, which in this case is a stationary RFID tag. Data is collected by RFID readers and antennas. In [1] - [3], the received signal power, or Received Signal Strength Indicator (RSSI) is used. RSSI measurements, however, are extremely ambiguous due to fading. Thus, Phase Of Arrival (POA) methods are considered more reliable. A drawback of POA measurements is the 2π ambiguity: the measured POA is wrapped between two values. In most cases it is in $[0, 2\pi)$. To overcome this obstacle, *unwrapping* must be applied which, however, requires high tag read rate. In [4] - [5], wrapped POA measurements are used along with the position of the measuring agent. In [6] - [8], 3D localization is achieved by using unwrapped POA measurement. A robot performing Simultaneous Localization And Mapping (SLAM) carries multiple antennas. A Synthetic Aperture Radar (SAR) algorithm is used to calculate the optimal position of the target. In [9], communicating with the target RFID tag in multiple frequency channels is shown to compensate for multipath effects, and locate the target; a method that cannot be applied in areas, with reduced bandwidth for UHF RFID systems, like Europe. In [10], a method to calculate the distance and bearing of the target relative to a mobile robot's pose is described. An Extended Kalman Filter (EKF) is used to fuse POA and robot odometry measurements. A handheld measuring system is presented in [11]. An Inertial Measuring Unit (IMU) is used to calculate the user's position as POA measurements are collected. In [12], a custom Multiple-Input Multiple-Output (MIMO) antenna built is mounted on a robot to collect POA and locate the target using a Particle Filter (PF) algorithm. In [13], PFs are used, but in this case along with Commercial Off The Shelf (COTS) RFID equipment. In [14], POA measurements and a Particle Swarm Optimization (PSO) algorithm are used to estimate the target's position. In [15] - [16], a RFID technology equipped robot is the mobile agent, collecting and leveraging both RSSI and POA measurements to achieve localization.

In [17], various indoor positioning technologies are presented, e.g. infrared radiation, vision-based systems, inertial navigation systems, ultrasound localization, Bluetooth and Wi-Fi. In [18], Wi-Fi and IMU sensor data are usde to calculate the position of the user in a camera-created 3D map. In [19] - [21], navigation instructions are provided to the user via Augmented

Reality (AR) technology.

In this paper we propose the design and functionality of a mobile handheld human-operated RFID reader used to locate a target RFID tag, improving our work presented in [22]. POA data collected by an RFID reader and rotation data measured by an IMU are fused to calculate the position of the target relatively to the user's current pose. A PF algorithm is used to improve the estimation as more iterations are completed.

In section II, the proposed method is presented. In section III, we describe the conducted experiments, and show the corresponding localization results. Finally, in section IV, conclusions and future work are discussed.

II. Proposed Method

The main components of the proposed handheld measuring device are two:

- An RFID reader connected to one antenna, communicating with the desired RFID tag target.
- A 9 Degrees of Freedom (9DoF) IMU, measuring angle around a given axis; in our case the axis perpendicular to the ground.

Fig. 1. Photograph of a prototype of the proposed device. The device is held so that the antenna is pointing in front of the user, and performs a "scanning" movement, as explained in section II. The target estimation appears as a red dot on the device's display, where the distance and the direction to it are indicated.

Fig. 1 shows an implementation of the proposed device.

Operating the device requires the consecutive executions of the following types of "commands":

- SCAN command: The user is required to "scan" the area in front using the device. Using the part of the arm from the elbow to the hand, the user moves the device on a plane parallel to the ground. During this motion POA and angle measurements are collected.
- TURN command: The user is required to rotate around the current pose, measuring the rotation using the IMU.
- MOVE command: The user is required to step forward holding the device straight ahead, collecting POA measurements. The displacement of the user is estimated based on these measurements.

Leveraging a PF algorithm, consecutive executions of the three commands are used to improve the estimation of the distance and direction of the target RFID tag, as explained in section II-B.

A. Measured Data

Data are collected by an RFID reader and a 9DoF IMU. The RFID reader measures POA which is wrapped in $[0, \pi)$. The high read rate allows us to perform phase unwrapping. Real measurements also include noise, which is modeled as a normally distributed variable. The measured phase is:

$$\phi_{meas} = (\phi + \phi_{noise}) \ \ mod \ \ (\pi) \tag{1}$$

$$\phi = \phi_p + \phi_o \tag{2}$$

$$\phi_p = \frac{4\pi}{\lambda} d \tag{3}$$

$$\phi_{noise} \sim N(0, s_{phase}), \tag{4}$$

where ϕ is the phase of the received signal, ϕ_p is the phase accumulated due to the electromagnetic wave propagation, ϕ_o is a phase offset including phases of the cables and the related hardware, ϕ_{noise} is the phase measurement noise, λ is the wavelength of the electromagnetic field, and d is the distance from the antenna to the tag.

The IMU measures the angle around the axis perpendicular to the ground. The measurements are in $[0, 2\pi)$, and unwrapping is required. Additionally, they include noise originating from the IMU as well as the user. Let the angle measured by the IMU be:

$$\theta_{meas} = (\theta + \theta_{noise}) \ \ mod \ (2\pi) \tag{5}$$

$$\theta_{noise} \sim N(0, s_{angle}), \tag{6}$$

where θ is the real angle, and θ_{noise} is the measurement's noise.

B. Particle Filter Algorithm

In this section we present the implemented PF algorithm. As explained in section II, the algorithm requires consecutive execution of SCAN, TURN, and MOVE commands.

1) SCAN Command: Initially, M particles are randomly generated. Particle p_m^l is the m-th of M particles during the l-th iteration. They represent a possible user pose relative to the target $\mathbf{T}_{ar} = [0, 0]$. p_m^l is defined by the following values:

- $\mathbf{K}_m^l = [x_m^l, y_m^l]$ are the user's coordinates on the xy-plane.
- $\bar{\mathbf{V}}_m^l$ is a complex number representing the direction on the xy-plain the user is facing to.
- a_m^l is the device rotation radius of the user, that is the length of the moving part of the user's arm as the scanning motion explained in section II is executed.
- w_m^l is the weight assigned to the particle. All particle weights are initially equal to 1.

After the initialization, the iterative process begins. A SCAN command is executed. This results to measurement set $Meas^l$ consisting of phase and rotation angle measurements:

$$Meas^l = \left[\phi_n^l, rot_n^l\right], \; n = 1, \ldots, N \tag{7}$$

ϕ_n^l and rot_n^l are the N pairs of phase and rotation angle measurements indicated by n during the l-th iteration. Using the rotation angle measurements, the positions $\mathbf{Q}_{m,n}^l$ of the device during the scan that correspond to each particle p_m^l can be calculated. An illustration of $\mathbf{Q}_{m,n}^l$ points of different particles p_m^l is shown in Fig. 2.

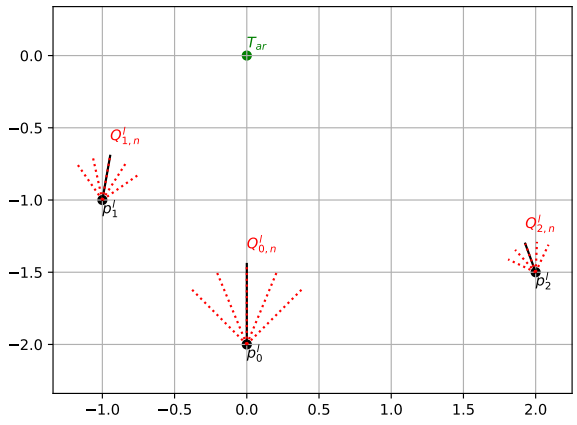

Fig. 2. $\mathbf{Q}_{m,n}^l$ points of different particles p_m^l, $m = 1, 2, 3$. The black line segments starting from the particle centers $\mathbf{K}_m^l$ indicate the direction of $\mathbf{V}_m^l$, and its length is equal to a_m^l. Their endpoints represent the assumed initial position of the device. The measured rotation angles rot_n^l, $n = 1, \ldots, 5$ are used to calculate points $\mathbf{Q}_{m,n}^l$ for each particle: the the device is rotate around the particle's center according to the measurements. $\mathbf{T}_{ar}$ is assumed position of the target.

A new normalized weight h_m^l for each particle p_m is calculated:

$$h_m^l = \frac{w_m^l / g_{cost}(m, l)}{\sum_{q=1}^{M} w_q^l / g_{cost}(q, l)} \tag{8}$$

$$g_{cost}(m, l) = \sum_{i=1}^{N} \sum_{j=i+1}^{N} \left(\Delta\phi_{i,j}^l - \Delta|\mathbf{T}_{ar}\mathbf{Q}_m|_{i,j}^l\right)^2 \tag{9}$$

$$\Delta\phi_{i,j}^l = \phi_i^l - \phi_j^l \tag{10}$$

$$\begin{aligned} \Delta|\mathbf{T}_{ar}\mathbf{Q}_m|_{i,j}^l = &\frac{4\pi}{\lambda}\left(||\mathbf{T}_{ar} - \mathbf{Q}_{m,i}^l||_2\right) \\ &-\frac{4\pi}{\lambda}\left(||\mathbf{T}_{ar} - \mathbf{Q}_{m,j}^l||_2\right) \end{aligned} \tag{11}$$

The theoretical phase difference is calculated in (11). Equation (10) is the measured phase difference. g_{cost} evaluates the similarity of theoretical phase difference and measured phase difference assuming that the user's position, facing direction, and rotation radius were those of particle p_m^l: $\mathbf{K}_m^l$, $\bar{\mathbf{V}}_m^l$, a_m^l. Finally, in (8) the weight value of the particle is divided by the value of the cost function $g_{cost}(m, l)$, and is normalized so that the sum of the normalized weight h_m^l is 1. Low g_{cost} function values correspond to lower error estimations. So, low $g_{cost}(m, l)$ values correspond to higher h_m^l values.

Having assigned normalized weights to all particles, the one with the highest normalized weight is used to estimate the target's position:

$$b^l = \arg\max_m \left(h_m^l\right) \tag{12}$$

$$D_{est}^l = ||\mathbf{K}_{b^l}^l - \mathbf{T}_{ar}||_2 \tag{13}$$

$$A_{est}^l = \angle\left(\mathbf{K}_{b^l}^l \bar{\mathbf{T}}_{ar}\right) - \angle\left(\bar{\mathbf{V}}_{b^l}^l\right) \tag{14}$$

Equation (13) is the distance of the b^l-th particle's center to the assumed target position, and (14) is the angle difference between the vector from the particle's center to the assumed target (which is the direction of the target, if the user was standing on the particle's position) and the particle's direction $\bar{\mathbf{V}}_{b^l}^l$.

If D_{est}^l is lower than a threshold D_{thresh}, the iterative process is finished.

2) TURN Command: The user is asked to rotate around the current position towards the estimated target. As the user rotates, new rotation angle measurements are collected. By comparing the unwrapped initial and final angle measurements, the turn angle $turn^l$ can be calculated. Every particle's $\bar{\mathbf{V}}_m^l$ value is updated according to $turn^l$.

3) MOVE Command: The user is asked to move straight ahead, towards the facing direction. The unwrapped phase difference $\Delta\phi_{step}^l$ between the final and initial position is measured and used to calculate the move distance of each particle. We update the particle center values accordingly.

4) Resampling: The aim of resampling is to replace the current particles with new ones. Since the particle with the highest weight is used to estimate the target, we want the new particles to be similar to high-weight particles. h_m^l values are used to create a probability distribution to pick particles for the next iteration. The practice called *jittering* is applied: Multiple copies of the same particle can be chosen for the next iteration. Jittering increases the diversity of the chosen particles, as shown in Fig. 3.

Then, the iterative process is repeated.

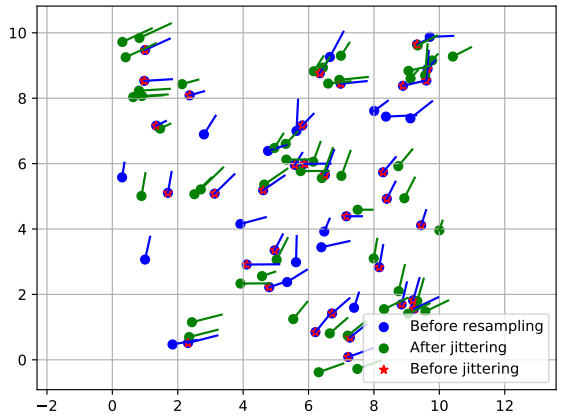

Fig. 3. Illustration of the resampling process. The dots represent the position $\mathbf{K}_m^l$ of the particles, the lines the direction $\bar{\mathbf{V}}_m^l$, and the length of each line the corresponding rotation radius a_m^l. The old blue particles are being resampled. The particles resampled at least once are marked red. The green ones are the new particle set, after jittering.

III. Experimental Results

Three experiments are presented. In all of them the user moves in a straight line. However, the original distance and orientation relative to the target is different. This allows us to evaluate both the distance and angle estimation accuracy. An illustration of the user's movement during each experiment is shown in Fig. 4. The distance and angle estimation expected absolute errors are shown in Table I. The following parameter values were used: $M = 1000$, $N = 20$. The mean angle estimation error is $\sim 4^o$, which is more than satisfactory considering the average human user's perception of rotation angle.

As for the distance estimation, in Experiments 1 and 2, it is unsuccessful. In these cases the angle between the target's direction and the user's facing direction increases as more steps are completed. This results to the trajectory of the antenna during the scanning motion to resemble a linear trajectory on a line parallel to the direction the target. This, however, maximizes the POA measurement ambiguity. Successful SAR methods rely on measurements collected on the complete opposite, that is trajectories perpendicular to the direction of the target.

In Experiment 3, the user moves towards the target, and more favorable measurement conditions are met. Now, after just two iterations of the algorithm, the distance is accurately estimated, and continues to do so in the following steps. The maximum error value is $0.45m$. Considering the accuracy of the target's a) angle estimation, and b) distance estimation when the user moves towards it, we conclude that if the user follows the device's instructions as to in which direction to move, the distance estimation will also be accurate.

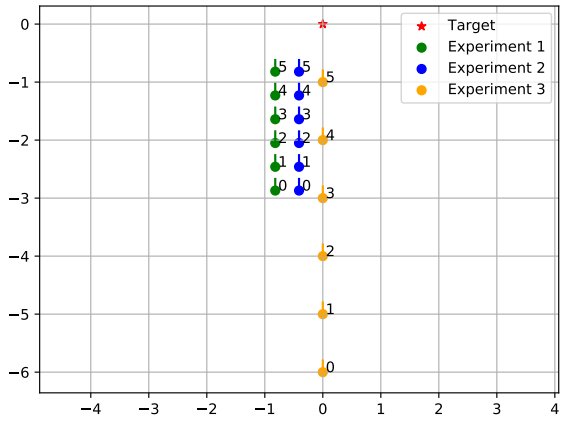

Fig. 4. Top view illustration of experiment user poses. The red marker is the position of the target. Each of the remaining colors represent one experiment: the dots show the position of the user, and the line segments the direction the user is facing to in the corresponding position. The numbers next to each pose indicate the chronological order of the poses in the corresponding experiment. Axis dimensions are in meters (m).

IV. Conclusions and Future Work

In this paper, we have presented a novel method for RFID tag localization using a handheld RFID reader. We also designed and implemented a prototype of the proposed handheld device. The user performs actions indicated by the device measuring POA and rotation angle. A PF algorithm fuses consecutive iteration measurements, and improves the target estimation. Experimental results showed high angle estimation accuracy of $\sim 4^o$. When the user was moving towards the target, as the device's instructions suggested, the distance estimation error was below $0.5m$ after just a couple of algorithm iterations.

Future work will be focused on improving the ease of use of the device, providing a fluid user friendly experience. The operation of the device's components can also be revamped to recognize and compensate for human related operation mistakes. Finally, more experiments must be conducted to evaluate the localization performance.

References

[1] S. Siachalou, A. Bletsas, J. Sahalos and A. G. Dimitriou, "RSSI-based maximum likelihood localization of passive RFID tags using a mobile cart," 2016 IEEE Wireless Power Transfer Conference (WPTC), 2016, pp. 1-4, doi: 10.1109/WPT.2016.7498847.

TABLE I
EXPERIMENT DISTANCE (M) AND ANGLE (DEG) ESTIMATIONS, AND CORRESPONDING ERRORS.

Experiment 1

	Distance (m)			Angle (deg)		
Index	Est.	G.T.	Error	Est.	G.T.	Error
0	1.31	3.18	-1.87	-18.1	-14.9	-3.2
1	2.20	2.79	-0.59	-22.4	-17.1	-5.3
2	4.13	2.40	1.73	-20.8	-20.0	-0.8
3	4.30	2.02	2.28	-19.0	-24.0	5.0
4	4.23	1.65	2.58	-20.9	-29.7	8.8
5	3.09	1.31	1.78	-34.0	-38.7	4.7

Experiment 2

	Distance (m)			Angle (deg)		
Index	Est.	G.T.	Error	Est.	G.T.	Error
0	7.96	3.10	4.86	-3.8	-7.6	3.8
1	2.89	2.70	0.19	-7.0	-8.7	1.7
2	2.36	2.29	0.07	-15.7	-10.3	-5.4
3	2.83	1.89	0.94	-13.2	-12.5	-0.7
4	2.90	1.49	1.41	-19.0	-15.9	-3.1
5	2.73	1.10	1.63	-19.3	-21.8	2.5

Experiment 3

	Distance (m)			Angle (deg)		
Index	Est.	G.T.	Error	Est.	G.T.	Error
0	1.73	6.00	-4.27	4.3	0	4.3
1	5.07	5.00	0.07	1.3	0	1.3
2	4.28	4.00	0.28	5.8	0	5.8
3	2.97	3.00	-0.03	-3.9	0	-3.9
4	2.45	2.00	0.45	-2.7	0	-2.7
5	1.40	1.00	0.4	-4.7	0	-4.7

*Est. := Estimation, G.T. := Ground Truth,
Error := Est. - G.T.

[2] D. Joho, C. Plagemann and W. Burgard, "Modeling RFID signal strength and tag detection for localization and mapping," 2009 IEEE International Conference on Robotics and Automation, 2009, pp. 3160-3165, doi: 10.1109/ROBOT.2009.5152372.

[3] J. Zhang, Y. Lyu, J. Patton, S. C. G. Periaswamy and T. Roppel, "BFVP: A Probabilistic UHF RFID Tag Localization Algorithm Using Bayesian Filter and a Variable Power RFID Model," in IEEE Transactions on Industrial Electronics, vol. 65, no. 10, pp. 8250-8259, Oct. 2018, doi: 10.1109/TIE.2018.2803720.

[4] A. Motroni, P. Nepa, P. Tripicchio and M. Unetti, "A Multi-Antenna SAR-based method for UHF RFID Tag Localization via UGV," 2018 IEEE International Conference on RFID Technology & Application (RFID-TA), 2018, pp. 1-6, doi: 10.1109/RFID-TA.2018.8552780.

[5] A. Motroni et al., "SAR-Based Indoor Localization of UHF-RFID Tags via Mobile Robot," 2018 International Conference on Indoor Positioning and Indoor Navigation (IPIN), 2018, pp. 1-8, doi: 10.1109/IPIN.2018.8533847.

[6] A. Tzitzis et al., "Localization of RFID Tags by a Moving Robot, via Phase Unwrapping and Non-Linear Optimization," in IEEE Journal of Radio Frequency Identification, vol. 3, no. 4, pp. 216-226, Dec. 2019, doi: 10.1109/JRFID.2019.2936969.

[7] A. Tzitzis, A. Raptopoulos Chatzistefanou, T. V. Yioultsis and A. G. Dimitriou, "A Real-Time Multi-Antenna SAR-Based Method for 3D Localization of RFID Tags by a Moving Robot," in IEEE Journal of Radio Frequency Identification, vol. 5, no. 2, pp. 207-221, June 2021, doi: 10.1109/JRFID.2021.3070409.

[8] A. Tzitzis, A. Malama, V. Drakaki, A. Bletsas, T. Yioultsis and A. G. Dimitriou, "Real-Time, Robot-Based, 3D Localization of RFID Tags, by Transforming Phase Measurements to a Linear Optimization Problem," in IEEE Journal of Radio Frequency Identification, doi: 10.1109/JRFID.2021.3103393.

[9] Longfei Shangguan and Kyle Jamieson. 2016. The Design and Implementation of a Mobile RFID Tag Sorting Robot. In Proceedings of the 14th Annual International Conference on Mobile Systems, Applications, and Services (MobiSys '16). Association for Computing Machinery, New York, NY, USA, 31–42. DOI:https://doi.org/10.1145/2906388.2906417

[10] E. DiGiampaolo and F. Martinelli, "Range and Bearing Estimation of an UHF-RFID Tag Using the Phase of the Backscattered Signal," in IEEE Journal of Radio Frequency Identification, vol. 4, no. 4, pp. 332-342, Dec. 2020, doi: 10.1109/JRFID.2020.3016168.

[11] K. Singh et al., "Localization of Life Safety Vests in an Aircraft Using Backscattering RFID Communication," in IEEE Journal of Radio Frequency Identification, vol. 4, no. 3, pp. 234-245, Sept. 2020, doi: 10.1109/JRFID.2020.3005248.

[12] M. Gareis, P. Fenske, C. Carlowitz and M. Vossiek, "Particle Filter-Based SAR Approach and Trajectory Optimization for Real-Time 3D UHF-RFID Tag Localization," 2020 IEEE International Conference on RFID (RFID), 2020, pp. 1-8, doi: 10.1109/RFID49298.2020.9244917.

[13] E. Giannelos, E. Andrianakis, K. Skyvalakis, A. G. Dimitriou and A. Bletsas, "Robust RFID Localization in Multipath With Phase-Based Particle Filtering and a Mobile Robot," in IEEE Journal of Radio Frequency Identification, vol. 5, no. 3, pp. 302-310, Sept. 2021, doi: 10.1109/JRFID.2021.3086759.

[14] F. Bernardini et al., "Particle Swarm Optimization in SAR-Based Method Enabling Real-Time 3D Positioning of UHF-RFID Tags," in IEEE Journal of Radio Frequency Identification, vol. 4, no. 4, pp. 300-313, Dec. 2020, doi: 10.1109/JRFID.2020.3005351.

[15] C. Li et al., "ReLoc: Hybrid RSSI- and Phase-Based Relative UHF-RFID Tag Localization With COTS Devices," in IEEE Transactions on Instrumentation and Measurement, vol. 69, no. 10, pp. 8613-8627, Oct. 2020, doi: 10.1109/TIM.2020.2991564.

[16] C. Li et al., "ReLoc 2.0: UHF-RFID Relative Localization for Drone-Based Inventory Management," in IEEE Transactions on Instrumentation and Measurement, vol. 70, pp. 1-13, 2021, Art no. 8003313, doi: 10.1109/TIM.2021.3069377.

[17] R. Mautz, "Indoor positioning technologies," Doctoral dissertation, Dept. Civil, Environ. Geomatic Eng., Inst. Geodesy Photogramm., ETH Zurich, Zurich, Switzerland, 2012

[18] P. Levchev, M. N. Krishnan, C. Yu, J. Menke and A. Zakhor, "Simultaneous fingerprinting and mapping for multimodal image and WiFi indoor positioning," 2014 International Conference on Indoor Positioning and Indoor Navigation (IPIN), 2014, pp. 442-450, doi: 10.1109/IPIN.2014.7275515.

[19] Gerstweiler G, Vonach E, Kaufmann H. HyMoTrack: A Mobile AR Navigation System for Complex Indoor Environments. Sensors (Basel). 2015 Dec 24;16(1):17. doi: 10.3390/s16010017. PMID: 26712755; PMCID: PMC4732050.

[20] U. Rehman and S. Cao, "Augmented-Reality-Based Indoor Navigation: A Comparative Analysis of Handheld Devices Versus Google Glass," in IEEE Transactions on Human-Machine Systems, vol. 47, no. 1, pp. 140-151, Feb. 2017, doi: 10.1109/THMS.2016.2620106.

[21] Mulloni, Alessandro & Seichter, Hartmut & Schmalstieg, Dieter. (2011). Handheld augmented reality indoor navigation with activity-based instructions. Mobile HCI 2011 - 13th International Conference on Human-Computer Interaction with Mobile Devices and Services. 211-220. 10.1145/2037373.2037406.

[22] A. Raptopoulos, T. Yioultsis and A. G. Dimitriou, "Particle Filter Object Tracking by a Handheld UHF RFID Reader," 2019 IEEE International Conference on RFID Technology and Applications (RFID-TA), 2019, pp. 342-347, doi: 10.1109/RFID-TA.2019.8892060.